

1 Internal variability vs multi-physics uncertainty in a  
2 regional climate model

3 A. Lavin-Gullon\*, J. Fernandez, S. Bastin, R. M. Cardoso,  
L. Fita, T. M. Giannaros, K. Goergen, J. M. Gutierrez,  
S. Kartsios, E. Katragkou, T. Lorenz, J. Milovac,  
P. M. M. Soares, S. Sobolowski, K. Warrach-Sagi

4 June 18, 2020

5 \*Corresponding author

6 A. Lavin-Gullon, J.M. Gutierrez  
7 Grupo de Meteorología. Instituto de Física de Cantabria (IFCA), CSIC-  
8 Universidad de Cantabria. Santander. Spain  
9 `alvaro.lavin@unican.es`  
10 J. Fernandez, J. Milovac  
11 Grupo de Meteorología y Computación. Dept. Matemática Aplicada y  
12 Ciencias de la Computación. Universidad de Cantabria. Santander. Spain  
13 T. Lorenz, S. Sobolowski  
14 NORCE Norwegian Research Centre, Bjerknes Centre for Climate Research,  
15 Bergen, Norway, S. Bastin  
16 LATMOS/IPSL, UVSQ Université Paris-Saclay, UPMC Univ. Paris 06,  
17 CNRS, Guyancourt, France  
18 L. Fita

19 Centro de Investigaciones del Mar y la Atmósfera (CIMA), CONICET-UBA,  
20 CNRS UMI-3351 IFAECI, C. A. Buenos Aires, Argentina  
21 K. Goergen  
22 Institute of Bio- and Geosciences (Agrosphere, IBG-3), Forschungszentrum  
23 Jülich (FZJ), Jülich, Germany  
24 E. Katragkou, S. Kartsios  
25 Department of Meteorology and Climatology, School of Geology, Aristotle  
26 University of Thessaloniki, Thessaloniki, Greece, R. M. Cardoso, P. M. M.  
27 Soares  
28 Instituto Dom Luiz, Faculdade de Ciências, Universidade de Lisboa, Lisbon,  
29 Portugal  
30 T. M. Giannaros  
31 National Observatory of Athens, Institute for Environmental Research and  
32 Sustainable Development, Athens, Greece  
33 K. Warrach-Sagi  
34 Institute of Physics and Meteorology (IPM), University of Hohenheim, Stuttgart,  
35 Germany

## Abstract

In a recent study, Coppola et al (2020) assessed the ability of an ensemble of convection-permitting models (CPM) to simulate deep convection using three case studies. The ensemble exhibited strong discrepancies between models, which were attributed to various factors. In order to shed some light on the issue, we quantify in this paper the uncertainty associated to different physical parameterizations from that of using different initial conditions, often referred to as the internal variability. For this purpose, we establish a framework to quantify both signals and we compare them for upper atmospheric circulation and near-surface variables. The analysis is carried out in the context of the CORDEX Flagship Pilot Study on Convective phenomena at high resolution over Europe and the Mediterranean, in which the intermediate RCM WRF simulations that serve to drive the CPM are run several times with different parameterizations. For atmospheric circulation (geopotential height), the sensitivity induced by multi-physics and the internal variability show comparable magnitudes and a similar spatial distribution pattern. For 2-meter temperature and 10-meter wind, the simulations with different parameterizations show larger differences than those launched with different initial conditions. The systematic effect over one year shows distinct patterns for the multi-physics and the internal variability. Therefore, the general lesson of this study is that internal variability should be analyzed in order to properly distinguish the impact of other sources of uncertainty, especially for short-term sensitivity simulations.

**Keywords:** Internal variability, Regional climate models, Uncertainty, Physical parameterizations, Ensemble

# 1 Introduction

The increasing resolution of Regional Climate Models (RCMs) has reached the so-called convection-permitting scale (Prein et al, 2015), by approaching resolutions of a few kilometers, typically used in Numerical Weather Prediction (NWP). A recent study by Coppola et al (2020) presented the largest multi-model ensemble of convection permitting RCMs to date, with an initial experiment exploring the ability of RCMs setup as NWP models and as regional climate modelling tools. Strong discrepancies between models were found in simulating three heavy precipitation events over the Alps. The explanation of these discrepancies was left open, and they speculated on three potential explanations: (1) the proximity of the event to the boundaries of the domain, (2) a failure in some RCMs to capture the response to the drivers of the event and (3) internal variability being responsible for the differences across models. This study is a follow up of Coppola et al (2020), where we investigate the role of internal variability in a selected event and we also further extend our analysis to a full annual cycle.

Internal, unforced climate variability is one of the main sources of uncertainty in global climate simulations (Hawkins and Sutton, 2009). Due to the non-linear and chaotic nature of the climate system, small perturbations to a given state of the system grow and develop different trajectories in the state space (Palmer, 2005). In a relatively short period of time, two slightly perturbed simulations in which initial conditions are modified can differ as much as two randomly chosen states of the climate system (Kalnay, 2003). When considering coupled systems that exhibit modes of low-frequency variability, even mean states over long periods of time can differ considerably. This internal or natural variability of the system is commonly explored using ensembles of simulations started from perturbed initial conditions (Haughton

et al, 2014). The uncertainty arising from internal variability is not negligible compared to other sources of uncertainty, such as GCM modelling or GHG-scenario uncertainty (Hawkins and Sutton, 2009; Deser et al, 2012; van Pelt et al, 2015; Kumar and Ganguly, 2018).

In contrast, internal variability emerging in regional climate models (RCMs) is usually smaller than that in GCMs (Caya and Biner, 2004). This uncertainty is also commonly assessed by using a multi-initial-conditions ensemble (MICE) in order to separate RCM internal variability from the signal of forced variability (Giorgi and Bi, 2000; Christensen et al, 2001; Caya and Biner, 2004; Lucas-Picher et al, 2008b; Giorgi, 2019; Bassett et al, 2020). Several studies concluded that at least 5-6 members should be considered to obtain robust estimates of internal variability (Lucas-Picher et al, 2008b; Laux et al, 2017). Recent studies (Bassett et al, 2020) point to the need of even larger ensembles. The amplification of perturbations in the initial conditions is damped somewhat by the continuous flow of information through the boundaries of the limited area domain. Lucas-Picher et al (2008a) quantified the relation between the RCM internal variability and the lateral boundary forcing over the domain. In mid-latitudes, internal variability has a seasonal behaviour with higher (lower) values in summer (winter), when the boundary forcing (e.g. storm track intensity) is weaker (stronger) and the model is more (less) free to develop its own circulation (Caya and Biner, 2004; Lucas-Picher et al, 2008b). According to the general atmospheric circulation, prevalent winds (e.g. westerlies in mid-latitudes) force a flow of information through the boundary. As a result, this forcing imposes a typical pattern that exhibits increasing internal variability as one travels downwind across the domain. Flow perturbations develop and grow as they travel through the RCM domain, reaching a maximum near the

117 downwind boundary where they are forced back to the flow of the GCM in  
118 the relaxation zone (Lucas-Picher et al, 2008b).

119 Despite its relevance, few studies have addressed other RCM uncertain-  
120 ties in the light of internal variability. Regarding multi-model uncertainty,  
121 Sanchez-Gomez et al (2009) explored the impact of internal variability for  
122 four different weather regimes, which showed different sensitivity depending  
123 on the lateral boundary conditions. The fraction of multi-model uncertainty  
124 in RCMs that can be explained by internal variability can be relatively large.  
125 For example, Gu et al (2018) suggest that it could be up to 70% of the to-  
126 tal uncertainty for the precipitation in Asia. Also, Fathalli et al (2019)  
127 reported that internal variability was comparable to the inter-model pre-  
128 cipitation spread in Tunisia during summertime, when the lateral forcing  
129 constraint is reduced. As for GCMs, the magnitude of RCM internal vari-  
130 ability depends on the synoptic circulation, model configuration, region and  
131 season (Giorgi and Bi, 2000; Alexandru et al, 2007).

132 The relevance of RCM internal variability is also recognized by the Coor-  
133 dinated Regional climate Downscaling Experiment (CORDEX; Giorgi and  
134 Gutowski, 2015), an international ongoing initiative endorsed by the World  
135 Climate Research Program which coordinates the regional climate downscal-  
136 ing community. Under this framework, multiple institutions are producing  
137 and analysing the largest regional multi-model ensemble in history, cover-  
138 ing all populated areas in the world with a standard set of continental-scale  
139 domains.

140 Multi-RCM ensembles sample the dynamical downscaling methodolog-  
141 ical uncertainty. As such, it is challenging to discern the contributions to  
142 uncertainty from other sources (e.g. physical process parameterizations, in-  
143 ternal variability). This is because RCMs developed by different groups

144 differ in so many aspects that the results from different models and mem-  
 145 bers cannot be used to understand the processes responsible for the spread.  
 146 There have been different attempts to decompose multi-model uncertainty  
 147 into other sources of uncertainty that can be more systematically explored.  
 148 Perturbed-Physics Ensembles (PPE; Yang and Arritt, 2002; Bellprat et al,  
 149 2012) consider a given RCM and explore the uncertainty associated to se-  
 150 lected parameters, by sweeping a range of acceptable parameter values. This  
 151 approach allows to link the resulting uncertainty to a specific parameter.  
 152 Multi-physics ensembles (MPE; see e.g. García-Díez et al, 2015) provide a  
 153 way to link modelling uncertainties to specific processes. These ensembles  
 154 are generated using a single RCM by switching between different alternative  
 155 physical parameterizations, which are the model components representing  
 156 sub-grid-scale processes such as cloud microphysics, radiation, turbulence,  
 157 etc. Physical parameterization are one of the key differences between dif-  
 158 ferent RCMs and, therefore, MPEs mimic multi-model ensembles with the  
 159 advantage of a fixed dynamical core and the rest of non-sampled physics  
 160 schemes. Of course, these fixed components also limit model diversity and,  
 161 therefore, MPEs cannot replace multi-model ensembles. Quite a few anal-  
 162 yses tested the ability of different MPEs to encompass the regional climate  
 163 in different areas (Fernández et al, 2007; Evans et al, 2012; Solman and  
 164 Pessacg, 2012; Jerez et al, 2013; García-Díez et al, 2015; Katragkou et al,  
 165 2015; Stegehuis et al, 2015; Devanand et al, 2018). Some of these analyses  
 166 mentioned internal variability as potential source of background noise that  
 167 impacts the sensitivity to the physical parameterization schemes (Tourpali  
 168 and Zanis, 2013; Stegehuis et al, 2015), though internal variability was not  
 169 formally investigated.

170 Few studies consider both physics sensitivity and internal variability. For

instance, Laux et al (2017) explicitly aim to separate the effects of internal variability from those of changes in land-use, suggesting that internal variability has a significant impact on precipitation. Crétat and Pohl (2012) also studied the effect of physical parameterizations on internal variability and questioned the robustness of previous physics sensitivity studies which did not take into account internal variability.

The Flagship Pilot Study on Convective phenomena at high resolution over Europe and the Mediterranean (FPS-Convection) is an ongoing initiative endorsed by CORDEX. This initiative aims at studying convective processes with CPM over the Alpine region (Coppola et al, 2020) by producing both multi-model and multi-physics ensembles of RCM simulations. The initial results showed large discrepancies between individual ensemble members in their representation of selected heavy precipitation events. In this work, we take advantage of the ensembles produced in the FPS-Convection to follow up the study of Coppola et al (2020), in which the origin of these discrepancies was determined out of the scope. Since causation is difficult to address in a multi-model approach, we focus on the multi-physics ensemble within the FPS-Convection RCMs that serve to drive the CPM. We quantitatively compare the signal arising from the use of different model components (physical parameterizations) against that associated to the background noise referred to internal variability at different time scales. The objective is twofold: (1) to assess whether modelling discrepancies in Coppola et al (2020) fall within the range of internal variability and (2) to quantify how much uncertainty in a multi-physics ensemble can be explained by internal variability.

The paper is structured as follows: The methodology and data used in this work are detailed in Section 2. Section 3 presents and discusses the



198 results. First, applied to a case study presented in Coppola et al. (2020) and,  
199 second, we extend the study to consider the role and relative magnitude of  
200 internal variability with respect to multi-physics uncertainty over an annual  
201 cycle. Finally, the conclusions are summarized in Section 4.

## 202 **2 Data & methods**

### 203 **2.1 Multi-physics ensemble**

204 In this work, we explore the uncertainty associated to physical parameteri-  
205 zations by using multi-physics ensembles (MPE, hereafter) generated in the  
206 context of the FPS-Convection. This initiative considers multiple RCMs,  
207 but here we will focus only on the sub-ensemble of simulations using the  
208 Weather Research and Forecasting (WRF) model (Skamarock et al, 2008).  
209 This modelling system provides the ability to switch among different physical  
210 parameterization schemes for a given sub-grid-scale process. Additionally,  
211 WRF allows for online telescopic nesting, running several nested domains si-  
212 multaneously and exchanging information across domains at each time step.  
213 This approach gives rise to much smaller artifacts close to the borders of  
214 the inner domains, as compared to the standard procedure of running the  
215 model offline, nested into the output of a coarser resolution domain.

216 All institutions participating in FPS-Convection and using WRF have  
217 coordinated a MPE by setting different physical configurations so that at  
218 least one option differs among them (Table 1). The MPE considers different  
219 options varying the parameterization schemes for cloud micro-physics pro-  
220 cesses, surface and land processes, planetary boundary layer, and radiative  
221 processes. All other model configuration and experimental setup are fixed,  
222 including the model version (ARW-WRF v3.8.1).

223 All FPS-Convection WRF simulations consider a high-resolution ( $\sim 3\text{km}$ ),  
 224 convection-permitting domain centered over the Alpine region (ALP-3) nested  
 225 into a coarser-resolution ( $\sim 12\text{ km}$ ), and much larger, pan-European domain.  
 226 Except for the deep convection parameterization scheme, that is switched off  
 227 in ALP-3, physical configuration does not differ between both domains. All  
 228 WRF ensemble members used one-way nesting, so there is no communica-  
 229 tion from the convection-permitting back to the coarser domain. Therefore,  
 230 the convection-permitting inner domain did not alter in any way the results  
 231 for the pan-European domain used in this work. Our analyses focus only  
 232 on this pan-European domain, since we are interested in the uncertainty of  
 233 the synoptic conditions over Europe, which drive the needed moisture that  
 234 leads to unstable conditions over the Alpine area (see Section 3.1). The  
 235 ALP-3 domain is not large enough to alter significantly the large-scale syn-  
 236 optic conditions, so, in order to reproduce the case studies of Coppola et al  
 237 (2020) in the ALP-3 domain, the right sequence of observed events should  
 238 be preserved first in the pan-European domain forcing simulations.

239 We use WRF data from two different FPS-Convection experiments driven  
 240 by 6-hourly initial and lateral boundary conditions taken from the ERA-  
 241 Interim Reanalysis (Dee et al, 2011):

242 **Experiment A** is described in Coppola et al (2020) and consisted of a  
 243 preliminary test with all participating models, including WRF. Three heavy  
 244 precipitation events in the Alpine region were simulated in two modes, iden-  
 245 tified as “weather-like” and “climate mode”. Weather-like simulations were  
 246 started one day before the onset of the events, aiming at simulating the event  
 247 as closely as possible to the reality, aided by the predictability provided by  
 248 the initial conditions. As the proximity of the initial conditions constrains

the internal variability, we did not consider weather-like simulations in this study. Climate-mode simulations were started one month before the event, so that initial conditions were not a source of predictability in this case and the models were mainly driven by the lateral boundary conditions, which is typical in regional climate modeling. We focus on a single event that occurred around the 23<sup>rd</sup> June, 2009, and was covered by climate-mode simulations running for the period from 1<sup>st</sup> June to 1<sup>st</sup> July, 2009 (see Section 3.1). WRF members of the ensemble showed the largest differences in terms of predictability of this particular event. WRF simulations for this experiment used a pan-European domain at  $0.11^\circ \times 0.11^\circ$  horizontal resolution (EUR-11), corresponding to the official EURO-CORDEX domain setup.

**Experiment B** consists of RCM evaluation simulations covering a 15-year period starting in 1999. All the WRF simulations started using the same initial conditions, with soil states generated by a 1-year spin-up run (1998). As in experiment A, the WRF model contributed with a MPE. However, the physical parameterizations for this experiment were slightly adjusted with respect to those used in experiment A (see Table 1) in order to consider more complex physics schemes and to avoid uncertainties from the interaction between distinct PBL and surface layer schemes. It should be noted that WRF simulations for this experiment used a slightly coarser  $\sim 15$  km horizontal resolution (EUR-15) than those in Experiment A, covering the same domain. This change was motivated to comply with the recommended odd nesting ratios for telescopic domains (5:1 in this case, from EUR-15 to ALP-3), which avoids interpolation between the staggered Arakawa-C grids used. In this way, fluxes across nested domains are more accurate and computationally efficient. In this study we used the first year (1999) of these

275 simulations.

## 276 **2.2 Multi-initial-conditions ensemble**

277 A MICE was run to assess the role of internal variability in explaining the  
278 uncertainty developed by the MPE. We used WRF configurations AI and BI  
279 (see Table 1) to match the setup of experiments A and B, respectively, using  
280 a set of 6 different initial conditions. The set of perturbed initial conditions  
281 was generated using the lagged method (see e.g. Laux et al, 2017), i.e. by  
282 starting the simulations the day before (AI-r1), 2 days before (AI-r2), and so  
283 on, up to a 5-day lag (AI-r5). This is a simple way of perturbing the initial  
284 conditions while maintaining the physical consistency among variables. The  
285 extra simulated days are excluded, and we analyze only the period common  
286 to the MPE. The standard, no-lag runs AI and BI (say, AI-r0 and BI-r0)  
287 are part of both the 8-member MPE and this 6-member MICE.

288 We ran the 1-year MICE corresponding to experiment B (BI-r1 to BI-  
289 r5) only for the EUR-15 domain, without the inner ALP-3 nesting, so as to  
290 significantly reduce computational demands. Since no feedback from ALP-  
291 3 back to EUR-15 was allowed in the MPE, our EUR-15 MICE is fully  
292 comparable to EUR-15 MPE.

## 293 **2.3 Quantification of uncertainty**

294 In order to quantify the uncertainty (spread) in the two ensembles, we fol-  
295 lowed the approach of Lucas-Picher et al (2008b), who used an unbiased  
296 estimator of the inter-member variance:

$$\sigma_X^2(s, t) = \frac{1}{M-1} \sum_{m=1}^M (X(s, t, m) - \langle X \rangle(s, t))^2 \quad (1)$$

297 where  $X(s, t, m)$  is the value of a given variable  $X$  at position  $s$  (summariz-  
 298 ing, in this case, typical bi-dimensional position indices  $i, j$ ), at time step  $t$   
 299 and from ensemble member  $m$ .  $M$  is the total number of ensemble members.  
 300 The term  $\langle X \rangle(s, t)$  is the ensemble mean at a given position  $s$  and time  $t$ :

$$\langle X \rangle(s, t) = \frac{1}{M} \sum_{m=1}^M X(s, t, m). \quad (2)$$

301 To avoid confusion, we keep in this methodological summary the notation  
 302 of Lucas-Picher et al (2008b) and earlier publications on internal variability,  
 303 although the use of Greek letters ( $\sigma^2$ ) to refer to a sample variance estimator  
 304 is uncommon, and usually reserved for the population parameters to be  
 305 estimated (Wilks, 2011). Note that even though this measure was proposed  
 306 to quantify internal variability, it is just a measure of spread or uncertainty,  
 307 that can be applied to any ensemble. This is typically employed to quantify  
 308 internal variability on MICE. In this work, we apply it to both MPE and  
 309 MICE.

310 The uncertainty, as represented by Eq. 1, is a spatio-temporal field. The  
 311 evolution of uncertainty in time ( $UT$ ) is calculated by considering the spatial  
 312 average of the inter-member variance  $\sigma_X^2$  as

$$UT^2 \equiv \overline{\sigma_X^2}^s(t) = \frac{1}{S} \sum_{s=1}^S \sigma_X^2(s, t) \quad (3)$$

313 where  $S$  is the total number of grid cells in the domain.  $UT^2$  represents the  
 314 domain average of the inter-member variance. To emphasize the quadratic  
 315 nature of this uncertainty measure, we use the symbol  $UT^2$  in Eq. 3 but, in  
 316 the following, we consider always its square root  $UT$ , which has the units  
 317 of the variable, and allows for an easier interpretation. In the same way, a  
 318 spatial distribution of the uncertainty ( $US$ ) is obtained by considering the

319 time average of the inter-member variance  $\sigma_X^2$  as

$$US^2 \equiv \overline{\sigma_X^2}^t(s) = \frac{1}{T} \sum_{t=1}^T \sigma_X^2(s, t) \quad (4)$$

320 where  $T$  is the total number of time steps in the period. This expression is  
 321 an estimate of the expected value of the inter-member variance over a period  
 322 of interest.

323 We consider transient eddy variability (*TEV*) as a reference for inter-  
 324 member variability. Passing weather systems create a natural time variabil-  
 325 ity in meteorological fields, which sets a limit to the maximum variability  
 326 attainable at a given location. This variability is seasonally dependent, so  
 327 Caya and Biner (2004) proposed to use a monthly estimator and compute a  
 328 spatial average to make it comparable to UT:

$$TEV^2 \equiv \hat{\sigma}_X^2(\tau, m) = \frac{1}{S} \sum_{s=1}^S \overline{\left( X(s, t, m) - \overline{X}^\tau(s, m) \right)^2}^\tau \quad (5)$$

329 where the  $\overline{\phantom{x}}^\tau$  operator computes the monthly average, i.e. the mean for all  
 330 time steps  $t$  corresponding to a given month  $\tau$ . Again, the  $\sigma$ -notation is from  
 331 previous literature but, in the following, we will simply refer to this monthly-  
 332 averaged, transient-eddy variance as TEV. Note that TEV depends on the  
 333 model and also suffers from sampling uncertainty, which will be quantified  
 334 by computing it from different ensemble members.

335 Finally, the long-term impact (*LTI*) of the inter-member uncertainty  
 336 on the climatology of a meteorological field is estimated by calculating the  
 337 variance of the climate among ensemble members as

$$LTI^2 \equiv \sigma_{\overline{X}}^2(s) = \frac{1}{M-1} \sum_{m=1}^M \left( \overline{X}^t(s, m) - \langle \overline{X}^t \rangle(s) \right)^2 \quad (6)$$

338 where  $\overline{X}^t(s, m)$  is the time average (i.e. the climatology) of each ensemble  
 339 member  $m$  and  $\langle \overline{X}^t \rangle(s)$  is the ensemble mean of the climatologies. Note  
 340 that LTI measures the "uncertainty" of climate, while US measures the  
 341 "climate" of the uncertainty. The latter is sensitive to the correspondence  
 342 of meteorological events (e.g. heavy precipitation convective events) in time  
 343 and space, while the former measures systematic deviations among members  
 344 that lead to a different mean state (climate).

### 345 **3 Results & discussion**

#### 346 **3.1 Event reproducibility**

347 As an example, we focus first on a heavy precipitation case study ana-  
 348 lyzed by Coppola et al (2020). The event was mostly driven by large-scale  
 349 features, which consisted of a cut-off low over the Balkans inducing a persis-  
 350 tent northeasterly flow over Austria. This unstable flow was warm and wet  
 351 enough to trigger extreme precipitation by orographic lifting upon reaching  
 352 the Alps. Observations reveal precipitation peaking on the 23<sup>rd</sup> June, 2009,  
 353 over Austria. RCM simulations consistently reproduced this heavy precipi-  
 354 tation event under weather-like initialization (see Section 2.1), but Coppola  
 355 et al (2020) reported mixed results when considering the climate-mode ini-  
 356 tialization. Some members of the multi-model/multi-physics ensemble com-  
 357 pletely missed the precipitation event or represent highly damped versions  
 358 of it (see Figure 4 of Coppola et al (2020)). They speculated on a poten-  
 359 tially weak background synoptic forcing for this event, which we investigate  
 360 in this work.

361 Notably, the WRF MPE alone also exhibited mixed results in reproduc-  
 362 ing the event. For illustration, Figure 1 (left) shows the accumulated pre-

363 precipitation on 23<sup>rd</sup> June for 4 WRF configurations. Only WRF configuration  
364 AF is able to reproduce the event, with extended precipitation over Austria.  
365 Other WRF configurations (AB, AE, AD) miss the event and show some  
366 precipitation over southern Italy or very scarce precipitation (configurations  
367 AC, AG, AI, not shown in Figure 1).

368 The synoptic situation, as represented by the 850hPa geopotential height  
369 (Figure 1, right), shows the cut-off low located as observed (ERA-Interim)  
370 over the Balkans for the AF configuration. For the rest of the MPE mem-  
371 bers, a low-pressure system is simulated in southern Italy, which alters the  
372 circulation so that the warm-moist airflow over the Alps is strongly reduced  
373 and precipitation is eventually not occurring or occurring over other areas  
374 (southern Italy).

375 Given that MPE members differ only in their physical parameterization  
376 schemes, one might be tempted to assume that configuration AF outper-  
377 forms the rest. That would imply e.g. that the use of the YSU non-local  
378 boundary layer scheme somehow helps in developing the cut-off low at the  
379 right location, as opposite to the MYNN2 local mixing scheme. This is the  
380 only difference between configurations AF and AD. Moreover, YSU alone  
381 cannot explain the ability of AF to represent the event, because configuration  
382 AB also used this PBL scheme. The only difference between configurations  
383 AF and AB is the land surface model (LSM). AF used Noah-MP, a much ex-  
384 tended version (Niu et al, 2011) of the Noah LSM (used in AB), considering  
385 a multi-layer snow model with more realistic snow physics, canopy shadows,  
386 snow on canopy, an aquifer layer, and many other improvements. Other con-  
387 figurations used Noah-MP (AD, AE or AI), though, and the low pressure  
388 system and precipitation still did not occur on the right place. Therefore,  
389 either the exact parameterization combination of configuration AF is the



key or there must be a different explanation for the discrepancies.

Note that WRF was run using one-way, online telescopic nesting and, therefore, we can also rule out the proximity of the high precipitation event to the ALP-3 domain boundaries as potential cause for the different model results in Coppola et al (2020). Boundary artifacts close to the inner boundaries are greatly reduced in this setup and still some WRF members reproduced the event while others missed it.

An alternative hypothesis is that the different development of the event in the different MPE members is just the result of internal variability. To test this hypothesis, we considered a MICE based on configuration AI, which did not develop the event under the standard MPE initialization setup (start date: 00UTC, 1<sup>st</sup> June, 2009). Configuration AI (AI-r0) developed a low over southern Italy (Figure 2a), as many of the other configurations (Figure 1). Many of the MICE members also developed a low over this area (see e.g. Figure 2), but member AI-r1 (start date: 00UTC, 31<sup>st</sup> May, 2009) presents a low in the right place, when compared against ERA-Interim. This was achieved by perturbing the initial conditions, starting the simulation one day earlier, and preserving exactly the same model configuration. Note that this is not a matter of improved initial conditions, since there are more than 20 days simulated from the geopotential height fields shown in Figures 1 (right) and 2, well beyond the limit of deterministic predictability of an atmospheric state. This is the result of internal variability. The slight perturbations in the initial conditions grew up by the non-linear dynamical model. This process is in competition with the constraints imposed by the lateral boundary conditions, which bring the flow towards that of ERA-Interim close to border of the domain. This constraint can be seen in Figures 1 (right) and 2.

417 In this particular flow state, there seem to be two preferred weather  
418 regimes over the southern Mediterranean area or, at least, our model sim-  
419 ulations were only able to generate these two weather regimes: one with  
420 a low evolving over southern Italy and the other with the low positioned  
421 over the Balkans. The observed flow took the Balkan low path even though  
422 the model has difficulties to reproduce this path. Note that these weather  
423 regimes and their probability of occurrence are likely model dependent. In  
424 any case, this is just one particular event. Once we have shown that internal  
425 variability can trigger flow deviations similar to those from different physi-  
426 cal parameterizations, we focus on quantifying their relative uncertainty, i.e.  
427 the spread of MPE and MICE ensembles.

428 The evolution of inter-member variance in time for MPE and MICE (Fig-  
429 ure 3) can reach comparable values. MPE member simulations take exactly  
430 the same initial and lateral boundary conditions from ERA-Interim, hence  
431 the uncertainty (essentially the member-to-member variability) at the start  
432 is very small (close to zero during the first day), indicating that all members  
433 produce similar circulation patterns. As the different physical parameteri-  
434 zations have an effect on the model, each member simulated a different syn-  
435 optic situation and the uncertainty increases. Regarding the MICE, since  
436 its members were initialized before the MPE start date shown in Figure  
437 3, the spread among members is larger than in the MPE in the beginning  
438 of June. MICE uncertainty (i.e. internal variability) remains fairly stable  
439 along the 1-month time span of the simulation. After about 10 days, the  
440 magnitude of MPE and MICE inter-member variance are comparable, with  
441 internal variability (MICE spread) generally larger than MPE spread. This  
442 suggests that the different physical parameterizations used in the MPE in-  
443 troduce smaller differences among members than those arising from internal

444 variability.

445 A qualitative look at the UT evolution (Figure 3) shows that, even if  
446 uncertainty remains quite stable, there are periods of increased uncertainty  
447 that seem to be synchronous in both ensembles. These must be periods of ei-  
448 ther weaker lateral boundary forcing (the only external forcing) or increased  
449 internal variability due to a particular situation of the internal dynamics.  
450 Notably, the period 22-26 June, when the heavy precipitation event occurred  
451 over Austria, is a period of increased uncertainty, where internal variabil-  
452 ity surpasses MPE spread. Also, MPE spread seems to develop a linear  
453 trend along the 1-month period. If sustained, this trend would overcome  
454 internal variability in longer periods. Unfortunately, FPS-Convection ex-  
455 periment A only considered 1-month-long simulations. In order to explore  
456 MPE vs. MICE uncertainty over a longer period, we use the output from  
457 FPS-Convection experiment B in the next section.

458 Experiment B produced a MPE with slightly different model configura-  
459 tions (Table 1) and also on a slightly coarser domain (EUR-15). In order to  
460 discard a sensitivity to this coarser resolution, we simulated a new MICE  
461 using AI configuration but on a much coarser  $0.44^\circ \times 0.44^\circ$  horizontal res-  
462 olution (EUR-44). Its spread (dashed line on Figure 3) is very similar to  
463 that of EUR-11, which suggests that a major part of the uncertainty is due  
464 to the large-scale synoptic pattern and not to smaller scale variability.

### 465 **3.2 Analysis over an annual cycle**

466 We extended the analysis to an one-year period taking advantage of FPS-  
467 Convection experiment B (Section 2.1). In particular, we extended Figure 3  
468 to one year using the year 1999 from the WRF MPE of experiment B and  
469 a MICE based on configuration BI. The resulting inter-member variance in

470 time (Figure 4) shows a very similar behaviour of MPE spread and inter-  
 471 nal variability (MICE spread) along the whole year. MPE members started  
 472 again from the same initial conditions. Therefore, they show very low dif-  
 473 ferences on January 1st, which increases after about 10 days. After this  
 474 10-day transient evolution affected by the initial conditions, both ensembles  
 475 show comparable inter-member variance, exhibiting an annual cycle with  
 476 increased uncertainty in summer. Moreover, even weekly to monthly vari-  
 477 ability in these UT time series seems to match in both ensembles. Notably  
 478 in the last months (Oct-Dec), and also in many other peaks along the year.  
 479 This suggests that the differences introduced by the different physics formu-  
 480 lations along the time are amplified by the model in a similar way than the  
 481 perturbations of the initial conditions. No systematic effect is noticeable in  
 482 the circulation. Put in another way, for this variable at least, multi-physics  
 483 uncertainty can be fully explained by internal variability.

484 As in previous studies (Caya and Biner, 2004; Lucas-Picher et al, 2008b),  
 485 we used transient-eddy variability (Equation 5) as a reference for uncer-  
 486 tainty. This is the natural variability of a meteorological field associated to  
 487 weather systems traveling along the storm track. TEV can be computed  
 488 from any of the ensemble members. We used simulation BI (top line in  
 489 Figure 4), which is the only member common to both MPE and MICE. To  
 490 evaluate the uncertainty associated to the selection of this particular mem-  
 491 ber, we computed the monthly TEV from each member, and its standard  
 492 deviation for each ensemble and for each month is shown as error bars in  
 493 Figure 4. TEV spread is very low and any member could have been used as  
 494 the reference. As already found in previous studies in mid-latitudes, TEV is  
 495 larger in winter than in summer, due to the more frequent passage of weather  
 496 systems from the Atlantic. The faster atmospheric circulation in winter im-

497 poses a strong boundary forcing, which may explain the lower spread among  
 498 ensemble members. TEV and the associated boundary forcing is lower dur-  
 499 ing summer. As a result, the model has more freedom to develop its own  
 500 circulation features, increasing the spread between the members. During  
 501 summer, the spread reaches approximately half of the TEV, which would be  
 502 the maximum attainable. This maximum is what one would expect from a  
 503 GCM, which has no lateral boundary constraints. For such a model, MICE  
 504 spread (i.e. internal variability) would increase during 1-2 weeks to reach  
 505 the TEV line and remain around this limit along the year. In this sense,  
 506 RCM internal variability is negligible compared to GCM internal variability  
 507 during winter, but it represents an important fraction (approximately one  
 508 half, in this example) during summer.

509 The similarity between MPE and MICE uncertainty is not restricted  
 510 to domain averages. In Figure 5, we show the spread in space, by averag-  
 511 ing inter-member variance in time for each model grid point (Equation 4).  
 512 Both maps show a typical spatial distribution of internal variability in mid-  
 513 latitudes, with increasing variability from the southwestern to the north-  
 514 eastern part of the domain. The patterns are remarkably similar, with  
 515 MPE inter-member variance (Figure 5a) only slightly larger than internal  
 516 variability (Figure 5b). Both reach about 35 m over the Baltic Sea and a  
 517 steeper gradient towards the outflow (eastern) boundary than in the inflow  
 518 (western) one. The westerly input flow is slowly modified by the RCM as it  
 519 travels along the domain, but it is suddenly modified at the outflow bound-  
 520 ary to match again the ERA-Interim flow at the eastern border. Christensen  
 521 et al (2001) suggested that, for a domain over Europe, the lower uncertainty  
 522 in south-western Europe is also due to the fact that the area is mainly sea,  
 523 and not only due to the distance to the boundaries. Seasonal winter (DJF)

524 and summer (JJA) patterns of MPE and MICE inter-member variance (not  
525 shown) are very similar to those in Figure 5. They show higher (lower)  
526 intensity in JJA (DJF), reaching 45 m (25 m) over the Baltic Sea.

527 The systematic effects of the physical parameterizations on the circu-  
528 lation can be seen in the long-term impact (Figure 6a). LTI summarizes  
529 the variability of the climatology for the different ensemble members (Equa-  
530 tion 6). Note that this variability is about one order of magnitude smaller  
531 than the uncertainty measures shown previously (cf. the scales of Figures 5  
532 and 6). Nevertheless, LTI has an impact on the simulated climate, while the  
533 (time) mean inter-member variance explored previously is mainly due to a  
534 lack of correlation (Caya and Biner, 2004). The largest differences among  
535 the simulations using different parameterizations occur in the center of the  
536 domain, between Germany and Poland, and extend towards the Alpine re-  
537 gion. Remarkably, systematic differences develop also on the northwestern  
538 boundary.

539 The LTI of internal variability (Figure 6b) shows a distinct pattern, with  
540 the largest values in the northern half of the domain. The magnitude is  
541 comparable to that of the MPE, though. Therefore, even though the spatial  
542 patterns are different, the systematic differences among MPE members are  
543 still comparable to the internal variability. This would suggest that one-year  
544 simulations are not enough to distinguish the systematic effect of a particular  
545 parameterization configuration compared to the impact of different initial  
546 conditions on the circulation. Since the MICE is just composed of multiple  
547 realizations of the same model configuration, its LTI must tend to zero as the  
548 simulation length increases and the climatology of all members tends towards  
549 the “true” model climatology. Longer simulations, such as those currently  
550 under way in the FPS-Convection, should provide a better assessment of

the LTI of the MPE. For example, for 10-year simulations, the values on Figure 6b should be divided by a factor of  $\sqrt{10} \approx 3.2$  (Lucas-Picher et al, 2008b). Up to this point, we have focused on the circulation (850 hPa geopotential height) and we have seen that multi-physics uncertainty is hard to distinguish from internal variability. The results for the circulation at 700 hPa or 500 hPa (not shown) are qualitatively similar.

### 3.3 Surface variables

Since circulation is only indirectly affected by physical parameterizations, in this section we focus on near-surface (2-meter) temperature. This is just one example of a variable affected by surface radiative and heat flux balances, which are parameterized in RCMs. In particular, the set of parameterizations tested in the FPS-Convection WRF ensemble (Table 1) directly affects cloud cover, surface energy (and mass) exchange and transport. As a result, this MPE shows a spread in surface temperature that substantially exceeds internal variability (Figure 7). Other near-surface variables, such as 10-meter wind, were also checked (not shown) and showed qualitatively similar results as near-surface temperature.

The evolution of inter-member variance for near-surface temperature, both for the MPE and MICE is different from the geopotential height shown in Figure 4. The annual cycle is clearer in the TEV than in the variance, which only shows a hint of a seasonal cycle during April through October. In summer, MPE and MICE spread evolution is uncorrelated, with some peak MPE uncertainty events (e.g. end of July) clearly standing out of internal variability. However, the strong winter variability seems coherent between MPE and MICE spread. Even if multi-physics spread is usually the greatest, internal variability seems to modulate it. This is in appar-

ent contradiction with the results of Cr  tat and Pohl (2012), who claimed that physical parameterizations modulate IV. They show that two MICE under different physical parameterization configurations develop a different amount of IV on average. However, they also show (their Figure 4b) a coherent evolution in time of the IV between model configurations. In our setup, physical parameterizations cannot modulate IV time evolution since the model configuration is fixed in the MICE. Still, Figure 7 shows that, despite the different spread amounts in MICE and MPE, both evolve coherently in time. It is likely that a third variable, such as the strength of the external forcing (i.e. boundary conditions), modulates the degree to which both physics and IV uncertainties can grow.

Transient-eddy variability for surface temperature (monthly step line in Figure 7) shows again the mid-latitude maximum during winter. A key difference compared to the geopotential height is the large variability of TEV within MPE members, as compared to the MICE members. In fact, uncertainty in MPE nearly doubles internal variability during some months. Notably, a peak uncertainty event by the end of July reaches the TEV line (especially, when considering its uncertainty), indicating that surface temperature patterns for the different physics differ as much as two random temperature patterns in this month. Note, however, that TEV was computed using a single month and, therefore, this estimate does not consider interannual variability. This might explain the reversal of the TEV cycle during November and December. The strong uncertainty in the November UT estimate is likely pushing up the TEV value for this month.

The spatial distribution of the inter-member variance for surface temperature (Figure 8) reveals, as before, a similar pattern of increasing spread towards the northeast in both ensembles. In this case, despite the similar



604 pattern, MPE shows larger spread values in accordance with Figure 7. MPE  
605 reaches a maximum value of about 3.5 K while MICE reaches about 2 K.

606 Finally, apart from the higher day-to-day uncertainty of the MPE for  
607 surface temperature, a systematic, long-term impact is clearly developed  
608 for this variable (Figure 9a). Unlike the circulation variable, the long-term  
609 impact of MPE for temperature is of comparable magnitude to its uncer-  
610 tainty. Also, it falls well above the long-term impact of internal variability  
611 (Figure 9b), suggesting that for variables directly influenced by physical pa-  
612 rameterizations (such as surface temperature), one-year simulations suffice  
613 to discern the systematic effect of a given parameterization with respect to  
614 another. Not only the magnitude, but also the spatial pattern of LTI differs  
615 between that of internal variability and the effect of parameterizations. The  
616 latter shows three main maxima over Africa, central Europe and Russia. As  
617 expected, impact is negligible over the sea, where surface temperatures are  
618 prescribed.

## 619 4 Conclusions

620 In this study we quantified the uncertainty arising from WRF model MPEs,  
621 on two different time scales, developed within the FPS-Convection interna-  
622 tional initiative. Additionally, for each MPE, new MICEs were performed  
623 to assess the role of internal variability in explaining the different ability  
624 of MPE members to reproduce specific convective events. The study was  
625 carried out for a one-month period focusing on a particular case study of  
626 heavy precipitation over Austria, and extended to one-year timescale.

627 The analyses over the one-month period already shed light on the 2 main  
628 objectives of this work: (1) The failure of some WRF model configurations to  
629 reproduce the case study, as reported by Coppola et al (2020), is not related

630 to physical parameterizations, but to the absence of a synoptic circulation  
631 pattern that favoured the event. Some members of the MICE were able  
632 to reasonably reproduce the observed synoptic pattern without modifying  
633 the model parameterization setup. (2) From a quantitative perspective, the  
634 spread due to the parameterization differences has a magnitude comparable  
635 to that from internal variability. Therefore, in these one-month simulations,  
636 the effect of the different physical parameterizations on the circulation can-  
637 not be distinguished from internal variability.

638 The extended study over a one-year period showed similar results for cir-  
639 culation variables (geopotential height). Multi-physics spread is comparable  
640 to internal variability both in its time evolution along the year and its spatial  
641 pattern. In this regard, we found multi-physics circulation uncertainty to  
642 behave according to previous RCM internal variability studies (Lucas-Picher  
643 et al, 2008b), with an annual cycle exhibiting increased uncertainty during  
644 summer and a spatial pattern of increased uncertainty towards the outflow  
645 boundaries of the regional domain.

646 The results, however, depend on the variable, with surface variables  
647 (known to be sensitive to parameterized processes) showing higher MPE  
648 spread. For example, for near-surface temperature the spread associated to  
649 parameterizations was above that due to the internal variability. This sug-  
650 gests that it is easier to discern both sources of uncertainties when analyzing  
651 variables more constrained by the model physics, which is typically the case  
652 in RCM parameterization sensitivity studies (Fernández et al, 2007; Evans  
653 et al, 2012; Solman and Pessacg, 2012; Jerez et al, 2013; García-Díez et al,  
654 2015; Katragkou et al, 2015; Stegehuis et al, 2015; Devanand et al, 2018).

655 As a reference for uncertainty, we computed transient-eddy variability,  
656 and quantified its spread due to the multi-physics and to internal variabil-

ity. This type of uncertainty also depends on the variable. For the circulation, transient-eddy variability of the different physical model configurations is similar to the internal variability range. However, for near-surface temperature, the different physics configurations exhibit a different level of transient-eddy variability. This requires further analysis on longer simulations to properly estimate the inter-annual contribution, but this is beyond the scope of the present work.

The long-term impact of the internal variability has been found to be of comparable magnitude to that of multi-physics for atmospheric circulation variables on year-long simulations. For surface temperature, however, the long-term impact of the multi-physics is larger, standing out of internal variability. For both variables, the spatial patterns of MPE and MICE differ, and this calls for a detailed study of each physical parameterization considered.

The techniques for quantification of internal variability (Lucas-Picher et al, 2008b) were applied here to explore also multi-physics spread, which proved to be a useful method for comparing both sources of uncertainty. They revealed that uncertainty arising from perturbations of the model physics (full replacement of a physics scheme) are seen from the circulation point of view as perturbations of initial conditions, i.e. as internal variability “noise”. Both types of perturbations seem amplified in a similar way by the dynamical system and synchronously constrained by the lateral boundary conditions. This view of a structured near-surface perturbation as a random upper air circulation noise was also found, in a completely different context, by Fernández et al (2009).

The inability of an RCM to reproduce the observed day-to-day circulation due to internal variability is not a matter of concern for mean cli-

684 mate studies, given that long-term climate is preserved (Caya and Biner,  
 685 2004). However, with the arrival of convection-permitting simulations and  
 686 the increasing interest in the climate of extremes, RCM internal variability  
 687 re-emerges as a matter of concern for model evaluation. As an example, the  
 688 FPS-Convection focuses on high-impact (low probability) convective phe-  
 689 nomena that occur mainly during the summer season, when lateral bound-  
 690 ary forcing is the weakest. The evaluation of models under these conditions  
 691 poses a real challenge that can only be addressed by computationally expen-  
 692 sive experiments including the simulation of long periods and/or the simula-  
 693 tion of a corresponding MICE to disentangle the role of internal variability  
 694 in the results. Other alternatives would be to constrain internal variability  
 695 by using techniques such as spectral nudging, which has its own drawbacks  
 696 (Alexandru et al, 2009), or frequently reinitializing the RCM (Lo et al, 2008;  
 697 Lucas-Picher et al, 2013).

698 Finally, the magnitude of internal variability in an RCM has been shown  
 699 to depend on the domain size and location (Giorgi and Bi, 2000; Rinke and  
 700 Dethloff, 2000; Alexandru et al, 2007). Given that, for circulation variables,  
 701 MPE variability behaves as internal variability, we could argue that a similar  
 702 dependence on domain size and location might affect MPE variability. The  
 703 generalization of these results for other domain sizes and for regions with a  
 704 weaker lateral boundary forcing is left for a forthcoming study.

## 705 **Acknowledgements**

706 This work is partially funded by the Spanish government through grant  
 707 BES-2016-078158 and MINECO/ FEDER co-funded projects INSIGNIA  
 708 (CGL2016-79210-R) and MULTI-SDM (CGL2015-66583-R). Universidad de  
 709 Cantabria simulations have been carried out on the Altamira Supercom-

puter at the Instituto de Física de Cantabria (IFCA-CSIC), member of the Spanish Supercomputing Network. EK and SK acknowledge the support of the Greek Research and Technology Network (GRNET) High Performance Computing (HPC) infrastructure for providing the computational resources of AUTH-simulations (under project ID pr003005) and the AUTH Scientific Computing Center for technical support. IPSL acknowledges the support from the EUCP project, funded by the European Union under H2020 Grant Agreement 776613, and from the IPSL mesocenter ESPRI facility which is supported by CNRS, UPMC, Labex L-IPSL, CNES and Ecole Polytechnique. IPSL simulations were granted access to the HPC resources of TGCC under the allocation A0050106877 made by GENCI. The computational resources for NORCE/BCCR were provided by UNINETT Sigma2 (NN9280K, NS9001K), with funding from the Research Council of Norway's support for the strategic project on climate services. FZJ gratefully acknowledges the computing time granted by the John von Neumann Institute for Computing (NIC) and JARA-HPC provided on the supercomputer JURECA at Jülich Supercomputing Centre (JSC). We acknowledge the E-OBS dataset from the EU-FP6 project UERRA (<https://www.uerra.eu>) and the Copernicus Climate Change Service, and the data providers in the ECA&D project (<https://eca.knmi.nl>).

## References

- Alexandru A, de Elia R, Laprise R (2007) Internal variability in regional climate downscaling at the seasonal scale. *Monthly Weather Review* 135(9):3221–3238, DOI 10.1175/MWR3456.1, URL <https://doi.org/10.1175/MWR3456.1>

735 Alexandru A, de Elia R, Laprise R, Separovic L, Biner S (2009) Sensitiv-  
736 ity study of regional climate model simulations to large-scale nudging  
737 parameters. *Monthly Weather Review* 137(5):1666–1686, DOI 10.1175/  
738 2008MWR2620.1

739 Bassett R, Young P, Blair G, Samreen F, Simm W (2020) A Large En-  
740 semble Approach to Quantifying Internal Model Variability Within the  
741 WRF Numerical Model. *Journal of Geophysical Research Atmospheres*  
742 125(7):e2019JD031,286, DOI 10.1029/2019JD031286

743 Bellprat O, Kotlarski S, Lüthi D, Schär C (2012) Exploring perturbed  
744 physics ensembles in a regional climate model. *Journal of Climate*  
745 25(13):4582–4599, DOI 10.1175/JCLI-D-11-00275.1

746 Caya D, Biner S (2004) Internal variability of RCM simulations  
747 over an annual cycle. *Climate Dynamics* 22(1):33–46, DOI 10.1007/  
748 s00382-003-0360-2

749 Christensen OB, Gaertner MA, Prego JA, Polcher J (2001) Internal variabil-  
750 ity of regional climate models. *Climate Dynamics* 17(11):875–887, DOI  
751 10.1007/s003820100154

752 Coppola E, Sobolowski S, Pichelli E, Raffaele F, Ahrens B, Anders I, Ban  
753 N, Bastin S, Belda M, Belusic D, Caldas-Alvarez A, Cardoso RM, Davo-  
754 lio S, Dobler A, Fernandez J, Fita L, Fumiere Q, Giorgi F, Goergen K,  
755 Güttler I, Halenka T, Heinzeller D, Hodnebrog Ø, Jacob D, Kartsios S,  
756 Katragkou E, Kendon E, Khodayar S, Kunstmann H, Knist S, Lavín-  
757 Gullón A, Lind P, Lorenz T, Maraun D, Marelle L, van Meijgaard E,  
758 Milovac J, Myhre G, Panitz HJ, Piazza M, Raffa M, Raub T, Rockel  
759 B, Schär C, Sieck K, Soares PMM, Somot S, Srnec L, Stocchi P, Tölle

760 MH, Truhetz H, Vautard R, de Vries H, Warrach-Sagi K (2020) A first-  
761 of-its-kind multi-model convection permitting ensemble for investigating  
762 convective phenomena over Europe and the Mediterranean. *Climate Dy-*  
763 *namics* DOI 10.1007/s00382-018-4521-8

764 Crétat J, Pohl B (2012) How physical parameterizations can modulate inter-  
765 nal variability in a Regional Climate Model. *Journal of the Atmospheric*  
766 *Sciences* 69(2):714–724, DOI 10.1175/JAS-D-11-0109.1

767 Dee DP, Uppala SM, Simmons AJ, Berrisford P, Poli P, Kobayashi S, An-  
768 drae U, Balmaseda MA, Balsamo G, Bauer P, Bechtold P, Beljaars ACM,  
769 van de Berg L, Bidlot J, Bormann N, Delsol C, Dragani R, Fuentes M,  
770 Geer AJ, Haimberger L, Healy SB, Hersbach H, Hlm EV, Isaksen L, Kll-  
771 berg P, Köhler M, Matricardi M, McNally AP, Monge-Sanz BM, Morcrette  
772 JJ, Park BK, Peubey C, de Rosnay P, Tavolato C, Thépaut JN, Vitart F  
773 (2011) The ERA-Interim reanalysis: configuration and performance of the  
774 data assimilation system. *Quarterly Journal of the Royal Meteorological*  
775 *Society* 137(656):553–597, DOI 10.1002/qj.828

776 Deser C, Phillips A, Bourdette V, Teng H (2012) Uncertainty in climate  
777 change projections: the role of internal variability. *Climate Dynamics*  
778 38(3):527–546, DOI 10.1007/s00382-010-0977-x

779 Devanand A, Ghosh S, Paul S, Karmakar S, Niyogi D (2018) Multi-  
780 ensemble regional simulation of Indian monsoon during contrasting rain-  
781 fall years: role of convective schemes and nested domain. *Climate Dynam-*  
782 *ics* 50(11):4127–4147, DOI 10.1007/s00382-017-3864-x

783 Evans JP, Ekström M, Ji F (2012) Evaluating the performance of a

784 WRF physics ensemble over South-East Australia. *Climate Dynamics*  
785 39(6):1241–1258, DOI 10.1007/s00382-011-1244-5

786 Fathalli B, Pohl B, Castel T, Safi MJ (2019) Errors and uncertainties in  
787 regional climate simulations of rainfall variability over Tunisia: a multi-  
788 model and multi-member approach. *Climate Dynamics* 52(1):335–361,  
789 DOI 10.1007/s00382-018-4150-2

790 Fernández J, Montávez J, Sáenz J, González-Rouco J, Zorita E (2007) Sen-  
791 sitivity of the MM5 mesoscale model to physical parameterizations for  
792 regional climate studies: Annual cycle. *Journal of Geophysical Research:*  
793 *Atmospheres* 112(D4)

794 Fernández J, Primo C, Cofiño AS, Gutiérrez JM, Rodríguez MA (2009) MVL  
795 spatiotemporal analysis for model intercomparison in EPS: application to  
796 the DEMETER multi-model ensemble. *Climate Dynamics* 33(2):233–243,  
797 DOI 10.1007/s00382-008-0456-9

798 García-Díez M, Fernández J, Vautard R (2015) An RCM multi-  
799 physics ensemble over Europe: multi-variable evaluation to avoid er-  
800 ror compensation. *Climate Dynamics* 45(11):3141–3156, DOI 10.1007/  
801 s00382-015-2529-x

802 Giorgi F (2019) Thirty years of regional climate modeling: Where are we and  
803 where are we going next? *Journal of Geophysical Research: Atmospheres*  
804 DOI 10.1029/2018JD030094

805 Giorgi F, Bi X (2000) A study of internal variability of a regional climate  
806 model. *Journal of Geophysical Research: Atmospheres* 105(D24):29,503–  
807 29,521, DOI 10.1029/2000JD900269



- 808 Giorgi F, Gutowski WJ (2015) Regional dynamical downscaling and the  
809 CORDEX initiative. *Annual Review of Environment and Resources*  
810 40(1):467–490, DOI 10.1146/annurev-environ-102014-021217
- 811 Gu H, Yu Z, Yang C, Ju Q, Yang T, Zhang D (2018) High-resolution en-  
812 semble projections and uncertainty assessment of regional climate change  
813 over China in CORDEX East Asia. *Hydrology and Earth System Sciences*  
814 22(5):3087–3103, DOI 10.5194/hess-22-3087-2018
- 815 Houghton N, Abramowitz G, Pitman A, Phipps SJ (2014) On the generation  
816 of climate model ensembles. *Climate Dynamics* 43(7):2297–2308, DOI  
817 10.1007/s00382-014-2054-3
- 818 Hawkins E, Sutton R (2009) The potential to narrow uncertainty in re-  
819 gional climate predictions. *Bulletin of the American Meteorological Soci-*  
820 *ety* 90(8):1095–1108, DOI 10.1175/2009BAMS2607.1
- 821 Haylock MR, Hofstra N, Klein Tank AMG, Klok EJ, Jones PD,  
822 New M (2008) A European daily high-resolution gridded data  
823 set of surface temperature and precipitation for 1950-2006. *Jour-*  
824 *nal of Geophysical Research: Atmospheres* 113(D20), DOI 10.1029/  
825 2008JD010201, URL [https://agupubs.onlinelibrary.wiley.com/](https://agupubs.onlinelibrary.wiley.com/doi/abs/10.1029/2008JD010201)  
826 [doi/abs/10.1029/2008JD010201](https://agupubs.onlinelibrary.wiley.com/doi/abs/10.1029/2008JD010201), [https://agupubs.onlinelibrary.](https://agupubs.onlinelibrary.wiley.com/doi/pdf/10.1029/2008JD010201)  
827 [wiley.com/doi/pdf/10.1029/2008JD010201](https://agupubs.onlinelibrary.wiley.com/doi/pdf/10.1029/2008JD010201)
- 828 Jerez S, Montavez JP, Gomez-Navarro JJ, Lorente-Plazas R, Garcia-Valero  
829 JA, Jimenez-Guerrero P (2013) A multi-physics ensemble of regional cli-  
830 mate change projections over the Iberian Peninsula. *Climate Dynamics*  
831 41(7):1749–1768, DOI 10.1007/s00382-012-1551-5

- 832 Kalnay E (2003) Atmospheric Modeling, Data Assimilation and Predictabil-  
833 ity. Cambridge University Press
- 834 Katragkou E, García-Díez M, Vautard R, Sobolowski S, Zanis P, Alexandri  
835 G, Cardoso RM, Colette A, Fernandez J, Gobiet A, Goergen K, Kara-  
836 costas T, Knist S, Mayer S, Soares PMM, Pytharoulis I, Tegoulis I, Tsik-  
837 erdekis A, Jacob D (2015) Regional climate hindcast simulations within  
838 EURO-CORDEX: evaluation of a WRF multi-physics ensemble. *Geosci-*  
839 *entific Model Development* 8(3):603–618, DOI 10.5194/gmd-8-603-2015
- 840 Kumar D, Ganguly AR (2018) Intercomparison of model response and  
841 internal variability across climate model ensembles. *Climate Dynamics*  
842 51(1):207–219, DOI 10.1007/s00382-017-3914-4
- 843 Laux P, Nguyen PNB, Cullmann J, Van TP, Kunstmann H (2017) How  
844 many RCM ensemble members provide confidence in the impact of land-  
845 use land cover change? *International Journal of Climatology* 37(4):2080–  
846 2100, DOI 10.1002/joc.4836
- 847 Lo JCF, Yang ZL, Pielke Sr RA (2008) Assessment of three dynamical cli-  
848 mate downscaling methods using the weather research and forecasting  
849 (WRF) model. *Journal of Geophysical Research: Atmospheres* 113(D9),  
850 DOI 10.1029/2007JD009216, URL [https://agupubs.onlinelibrary.](https://agupubs.onlinelibrary.wiley.com/doi/abs/10.1029/2007JD009216)  
851 [wiley.com/doi/abs/10.1029/2007JD009216](https://agupubs.onlinelibrary.wiley.com/doi/abs/10.1029/2007JD009216)
- 852 Lucas-Picher P, Caya D, Biner S, Laprise R (2008a) Quantification of  
853 the lateral boundary forcing of a Regional Climate Model using an ag-  
854 ing tracer. *Monthly Weather Review* 136(12):4980–4996, DOI 10.1175/  
855 2008MWR2448.1, URL <https://doi.org/10.1175/2008MWR2448.1>
- 856 Lucas-Picher P, Caya D, de Elía R, Laprise R (2008b) Investigation of re-

857 gional climate models' internal variability with a ten-member ensemble  
858 of 10-year simulations over a large domain. *Climate Dynamics* 31(7):927–  
859 940, DOI 10.1007/s00382-008-0384-8, URL <https://doi.org/10.1007/s00382-008-0384-8>  
860

861 Lucas-Picher P, Boberg F, Christensen JH, Berg P (2013) Dynamical  
862 downscaling with reinitializations: A method to generate finescale cli-  
863 mate datasets suitable for impact studies. *Journal of Hydrometeorol-*  
864 *ogy* 14(4):1159–1174, DOI 10.1175/JHM-D-12-063.1, URL <https://doi.org/10.1175/JHM-D-12-063.1>  
865

866 Niu GY, Yang ZL, Mitchell KE, Chen F, Ek MB, Barlage M, Kumar A,  
867 Manning K, Niyogi D, Rosero E, et al (2011) The community Noah land  
868 surface model with multiparameterization options (Noah-MP): 1. model  
869 description and evaluation with local-scale measurements. *Journal of Geo-*  
870 *physical Research: Atmospheres* 116(D12), DOI 10.1029/2010JD015139

871 Palmer T (2005) Global warming in a nonlinear climate. Can we be sure?  
872 *Europhysics news* 36(2):42–46

873 van Pelt SC, Beersma JJ, Buishand TA, van den Hurk BJJM, Schellekens J  
874 (2015) Uncertainty in the future change of extreme precipitation over the  
875 Rhine basin: the role of internal climate variability. *Climate Dynamics*  
876 44(7):1789–1800, DOI 10.1007/s00382-014-2312-4

877 Prein AF, Langhans W, Fosser G, Ferrone A, Ban N, Goergen K, Keller  
878 M, Tlle M, Gutjahr O, Feser F, Brisson E, Kollet S, Schmidli J, van  
879 Lipzig NPM, Leung R (2015) A review on regional convection-permitting  
880 climate modeling: Demonstrations, prospects, and challenges. *Reviews of*

881 Geophysics 53(2):323–361, DOI 10.1002/2014RG000475, URL [https://](https://agupubs.onlinelibrary.wiley.com/doi/abs/10.1002/2014RG000475)  
882 [agupubs.onlinelibrary.wiley.com/doi/abs/10.1002/2014RG000475](https://agupubs.onlinelibrary.wiley.com/doi/abs/10.1002/2014RG000475)

883 Rinke A, Dethloff K (2000) On the sensitivity of a regional Arctic climate  
884 model to initial and boundary conditions. *Climate Research* 14:101–113,  
885 DOI 10.3354/cr014101

886 Sanchez-Gomez E, Somot S, Déqué M (2009) Ability of an ensemble of re-  
887 gional climate models to reproduce weather regimes over Europe-Atlantic  
888 during the period 1961–2000. *Climate Dynamics* 33(5):723–736, DOI  
889 10.1007/s00382-008-0502-7

890 Skamarock WC, Klemp JB, Dudhia J, Gill DO, Barker M, Duda KG,  
891 Y Huang X, Wang W, Powers JG (2008) A description of the ad-  
892 vanced research WRF Version 3. NCAR Technical Note pp 1–113, DOI  
893 10.5065/D68S4MVH

894 Solman SA, Pessacg NL (2012) Regional climate simulations over South  
895 America: sensitivity to model physics and to the treatment of lateral  
896 boundary conditions using the MM5 model. *Climate Dynamics* 38(1):281–  
897 300, DOI 10.1007/s00382-011-1049-6

898 Stegehuis AI, Vautard R, Ciais P, Teuling AJ, Miralles DG, Wild M (2015)  
899 An observation-constrained multi-physics WRF ensemble for simulating  
900 european mega heat waves. *Geoscientific Model Development* 8(7):2285–  
901 2298, DOI 10.5194/gmd-8-2285-2015

902 Thompson G, Field PR, Rasmussen RM, Hall WD (2008) Explicit forecasts  
903 of winter precipitation using an improved bulk microphysics scheme. Part  
904 II: Implementation of a new snow parameterization. *Monthly Weather*  
905 *Review* 136(12):5095–5115, DOI 10.1175/2008MWR2387.1

906 Tourpali K, Zanis P (2013) Winter anticyclonic blocking effects over Europe  
 907 during 1960-2000 from an ensemble of regional climate models. Climate  
 908 Research 57:81–91, DOI 10.3354/cr01169

909 Wilks DS (2011) Statistical methods in the atmospheric sciences, vol 100.  
 910 Academic press

911 Yang Z, Arritt RW (2002) Tests of a Perturbed Physics Ensemble Approach  
 912 for Regional Climate Modeling. Journal of Climate 15(20):2881–2896,  
 913 DOI 10.1175/1520-0442(2002)015<2881:TOAPPE>2.0.CO;2,URL [https:](https://doi.org/10.1175/1520-0442(2002)015<2881:TOAPPE>2.0.CO;2)  
 914 [//doi.org/10.1175/1520-0442\(2002\)015<2881:TOAPPE>2.0.CO;2](https://doi.org/10.1175/1520-0442(2002)015<2881:TOAPPE>2.0.CO;2)

## 915 List of Tables

916	1	WRF multi-physics configurations considered in this study	
917		(see Section 2.1) for experiment A (one-month simulation,	
918		EUR-11 domain) and experiment B (one-year simulation, EUR-	
919		15). For each ensemble member, the table shows an Id. code,	
920		the institution performing the simulation and the physical	
921		parameterizations used. The ensembles explore the use of	
922		different schemes for micro-physics (MP), planetary bound-	
923		ary layer and surface layer (PBL), land surface (LSM), and	
924		shallow convection (ShC) processes. The PBL schemes de-	
925		noted with asterisk (*) used a different surface layer scheme	
926		despite sharing the MYNN2 PBL. See Table 2 for details of	
927		each parameterization scheme. . . . .	39
928	2	Physical schemes used in the multi-physics experiments shown	
929		in Table 1. . . . .	40

Exp.	Id.	Institution	MP	PBL	LSM	ShC
A	AB	Forschungszentrum Jülich (FZJ-IBG3), Germany	Thomp.	YSU	NOAH	GRIMS
	AC	National Observatory of Athens (NOA), Greece	Thomp.	MYNN2	NOAH	GRIMS
	AD	University of Hohenheim (UHOH), Germany	Thomp.	MYNN2*	NOAH-MP	GRIMS
	AE	Intitute Pierre Simon Laplace (IPSL), France	Thomp.	MYNN2	NOAH-MP	UW
	AF	Bjerknes Centre for Climate Res. (BCCR), Norway	Thomp.	YSU	NOAH-MP	GRIMS
	AG	Aristotle University of Thessaloniki (AUTH), Greece	WDM6	YSU	NOAH	GRIMS
	AH	Instituto Dom Luiz (IDL), Portugal	WDM6	MYNN2	NOAH	GRIMS
	AI	Universidad de Cantabria (UCAN), Spain	WDM6	MYNN2*	NOAH-MP	GRIMS
B	BB	Forschungszentrum Jülich (FZJ-IBG3), Germany	Th-AA	YSU	NOAH	GRIMS
	BC	National Observatory of Athens (NOA), Greece	Thomp.	MYNN2	NOAH	GRIMS
	BD	University of Hohenheim (UHOH), Germany	Th-AA	MYNN2	NOAH-MP	GRIMS
	BE	Intitute Pierre Simon Laplace (IPSL), France	Th-AA	MYNN2	NOAH-MP	UW
	BF	Bjerknes Centre for Climate Res. (BCCR), Norway	Thomp.	YSU	NOAH-MP	GRIMS
	BG	Aristotle University of Thessaloniki (AUTH), Greece	WDM6	YSU	NOAH-MP	GRIMS
	BH	Instituto Dom Luiz (IDL), Portugal	WDM6	MYNN2	NOAH	GRIMS
	BI	Universidad de Cantabria (UCAN), Spain	WDM6	MYNN2	NOAH-MP	GRIMS

Table 1: WRF multi-physics configurations considered in this study (see Section 2.1) for experiment A (one-month simulation, EUR-11 domain) and experiment B (one-year simulation, EUR-15). For each ensemble member, the table shows an Id. code, the institution performing the simulation and the physical parameterizations used. The ensembles explore the use of different schemes for micro-physics (MP), planetary boundary layer and surface layer (PBL), land surface (LSM), and shallow convection (ShC) processes. The PBL schemes denoted with asterisk (\*) used a different surface layer scheme despite sharing the MYNN2 PBL. See Table 2 for details of each parameterization scheme.

Acronym	Physical scheme
Thomp.	Thompson et al (2008) scheme with ice, snow and graupel processes suitable for high-resolution simulations
Th-AA	New Thompson aerosol-aware scheme considering water- and ice-friendly aerosols
WDM6	WRF Double-Moment 6-class microphysics scheme with cloud condensation nuclei for warm processes
YSU	Yonsei University non-local closure PBL scheme with revised MM5 Monin-Obukhov surface layer
MYNN2	Mellor-Yamada Nakanishi and Niino Level 2.5 (*combined with revised MM5 Monin-Obukhov surface layer)
NOAH	Noah LSM with multilayer soil temperature and moisture, snow cover and frozen soil physics
NOAH-MP	Noah LSM-Multi Physics. NOAH with multiple options for land-atmosphere processes
GRIMS	Shallow cumulus scheme from the Global/Regional Integrated Modeling System
UW	University of Washington shallow cumulus scheme from the Community Earth System Model

Table 2: Physical schemes used in the multi-physics experiments shown in Table 1.



## 930 List of Figures

931	1	Left: Accumulated precipitation (mm) on June, 23rd 2009	
932		according to E-OBS (Haylock et al (2008); top) and as simu-	
933		lated in the ALP-3 domain by experiment A for WRF MPE	
934		members AF, AD, AB and AE. Right: 850hPa geopotential	
935		height (m) according to ERA-Interim (top) and the corre-	
936		sponding MPE ensemble members in the EUR-11 domain in	
937		pink. An ERA-Interim 1500m-isoline (the same in all panels)	
938		is represented for reference in black. . . . .	42
939	2	As Figure 1 (right), but for 4 MICE members: AI-r0 to AI-r3.	43
940	3	Inter-member variance in time (Equation 3) for 850hPa geopo-	
941		tential height (m) in EUR-11 domain of experiment A (June	
942		2009). The spread is computed separately for MPE (blue)	
943		and MICE (red). The latter was computed both at $0.11^\circ$ and	
944		$0.44^\circ$ horizontal resolution with similar number of ensemble	
945		members. . . . .	44
946	4	Inter-member variance in time (UT) for 850hPa geopotential	
947		height (m) in EUR-15 domain of experiment B (year 1999).	
948		The uncertainty is computed separately for MPE (blue) and	
949		MICE (red). Transient-eddy variability (Equation 5, black	
950		line) was computed from BI configuration and error bars show	
951		its standard deviation for MPE and MICE. . . . .	45
952	5	Spatial distribution of the inter-member variance (US) for	
953		the 850 hPa geopotential height (m) in EUR-15 domain of	
954		experiment B (year 1999). a) multi-physics ensemble. b)	
955		multi-initial-conditions ensemble. . . . .	46
956	6	Long-term impact of multi-physics (a) and multi-initial-conditions	
957		(b) on 850hPa geopotential height (m). . . . .	47
958	7	As Fig. 4 but for surface temperature over land. . . . .	48
959	8	Spatial distribution of the inter-member variance for surface	
960		temperature (K) in EUR-15 domain of experiment B (year	
961		1999). a) multi-physics ensemble. b) multi-initial-conditions	
962		ensemble. . . . .	49
963	9	Long-term impact of multi-physics (a) and multi-initial-conditions	
964		(b) on surface temperature (K). . . . .	50

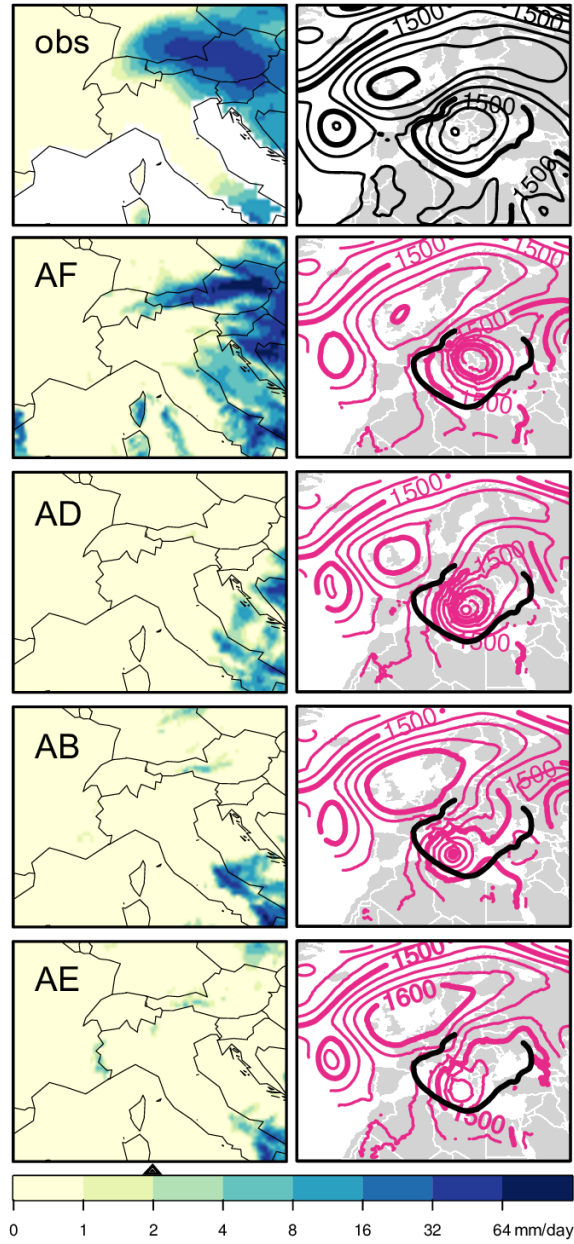


Figure 1: Left: Accumulated precipitation (mm) on June, 23rd 2009 according to E-OBS (Haylock et al (2008); top) and as simulated in the ALP-3 domain by experiment A for WRF MPE members AF, AD, AB and AE. Right: 850hPa geopotential height (m) according to ERA-Interim (top) and the corresponding MPE ensemble members in the EUR-11 domain in pink. An ERA-Interim 1500m-isoline (the same in all panels) is represented for reference in black.

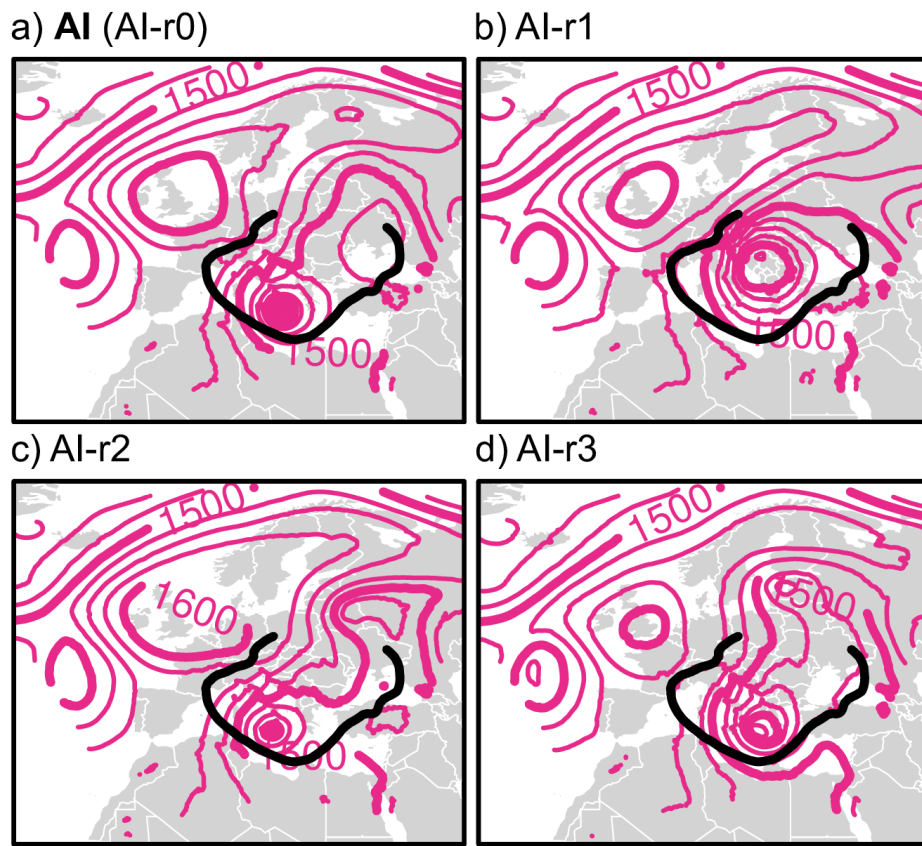


Figure 2: As Figure 1 (right), but for 4 MICE members: AI-r0 to AI-r3.

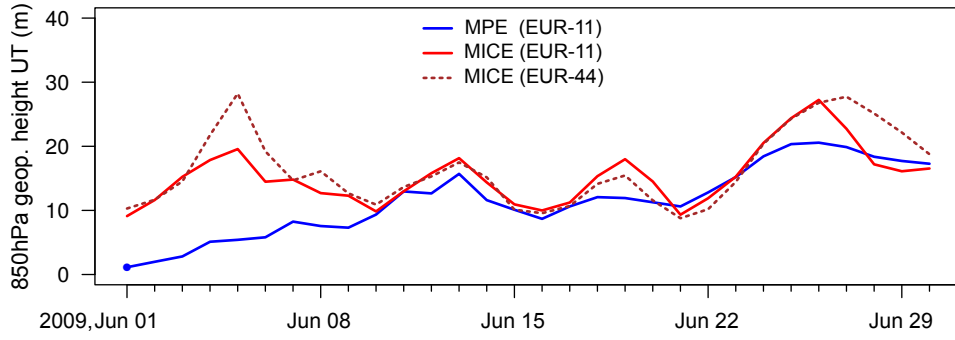


Figure 3: Inter-member variance in time (Equation 3) for 850hPa geopotential height (m) in EUR-11 domain of experiment A (June 2009). The spread is computed separately for MPE (blue) and MICE (red). The latter was computed both at  $0.11^\circ$  and  $0.44^\circ$  horizontal resolution with similar number of ensemble members.

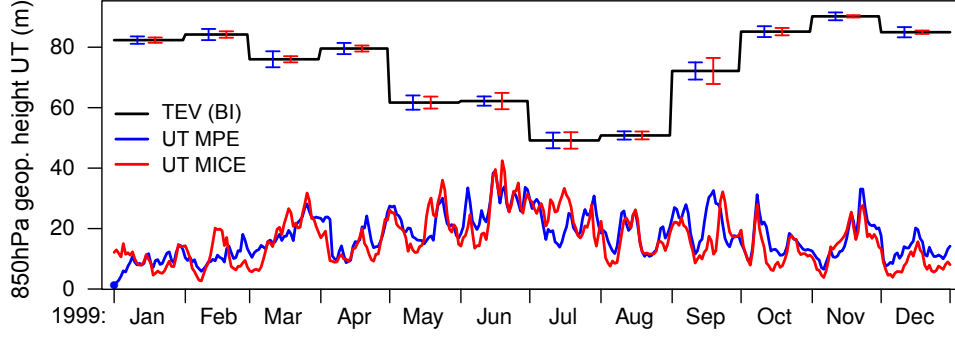


Figure 4: Inter-member variance in time (UT) for 850hPa geopotential height (m) in EUR-15 domain of experiment B (year 1999). The uncertainty is computed separately for MPE (blue) and MICE (red). Transient-eddy variability (Equation 5, black line) was computed from BI configuration and error bars show its standard deviation for MPE and MICE.

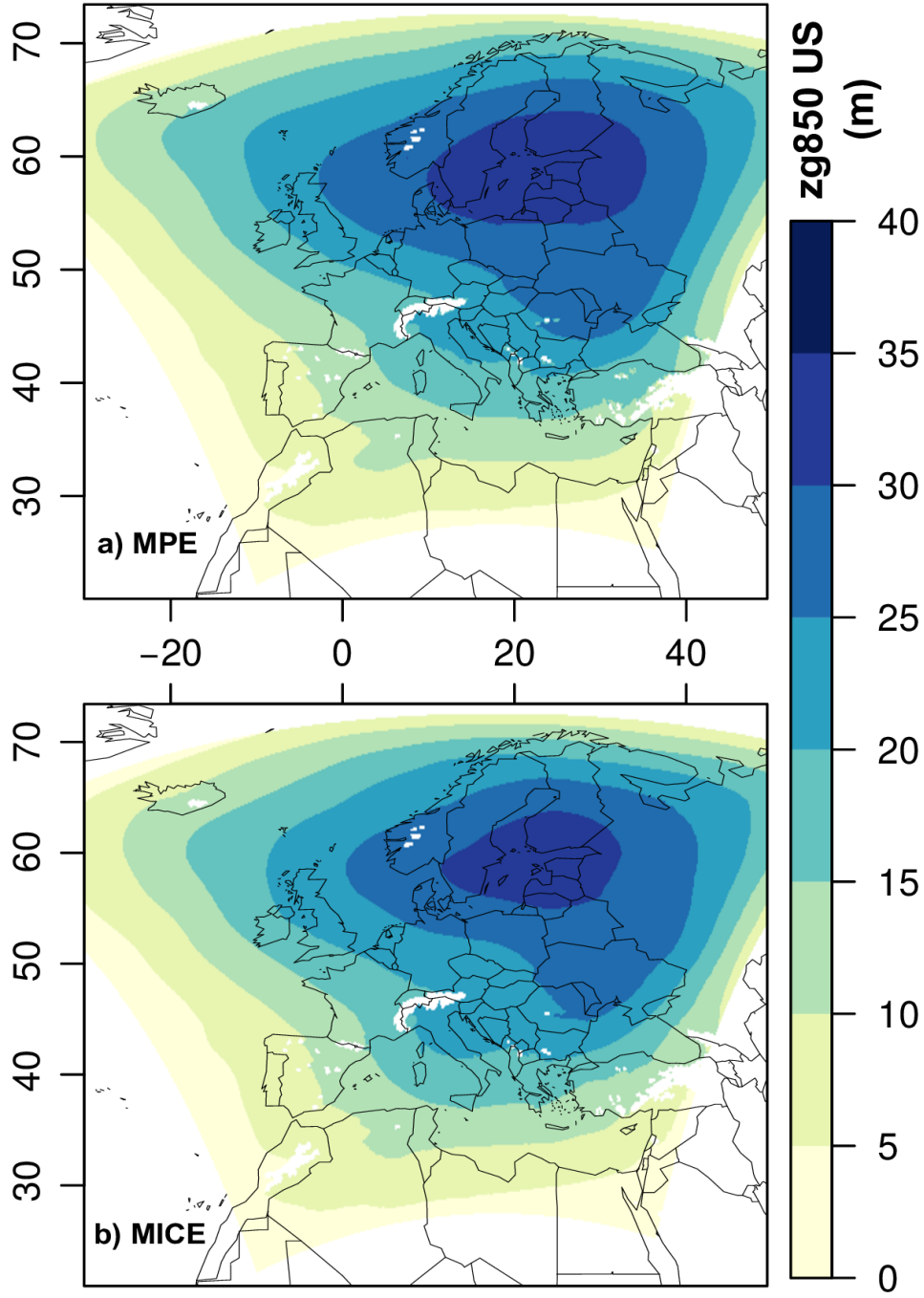


Figure 5: Spatial distribution of the inter-member variance (US) for the 850 hPa geopotential height (m) in EUR-15 domain of experiment B (year 1999). a) multi-physics ensemble. b) multi-initial-conditions ensemble.

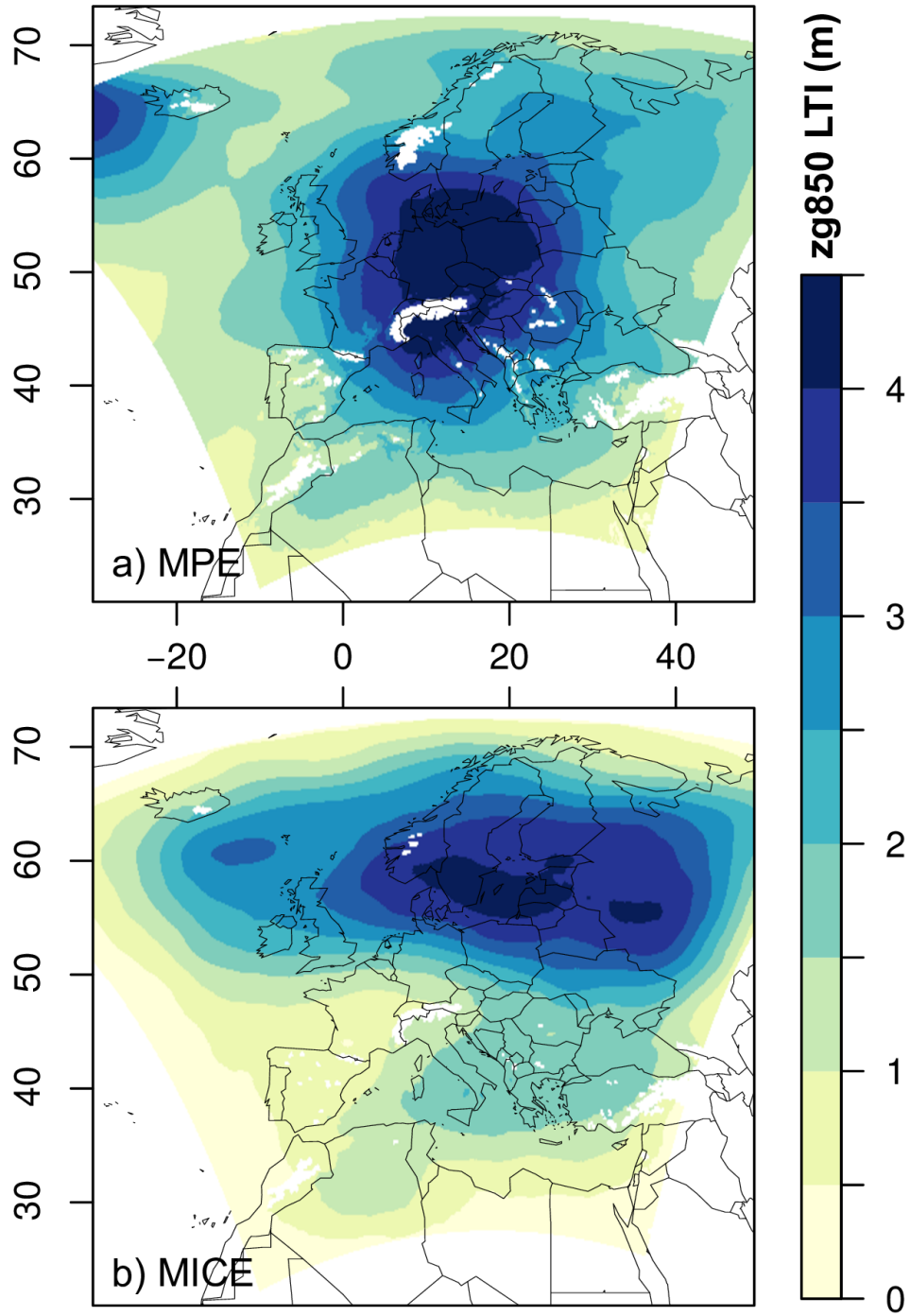


Figure 6: Long-term impact of multi-physics (a) and multi-initial-conditions (b) on 850hPa geopotential height (m).

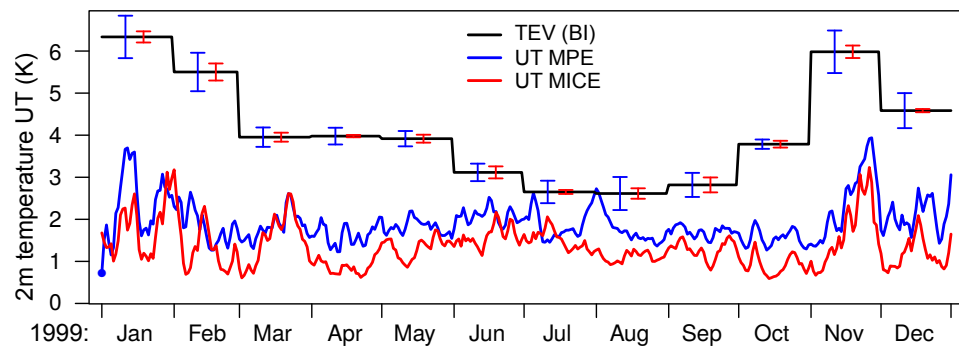


Figure 7: As Fig. 4 but for surface temperature over land.



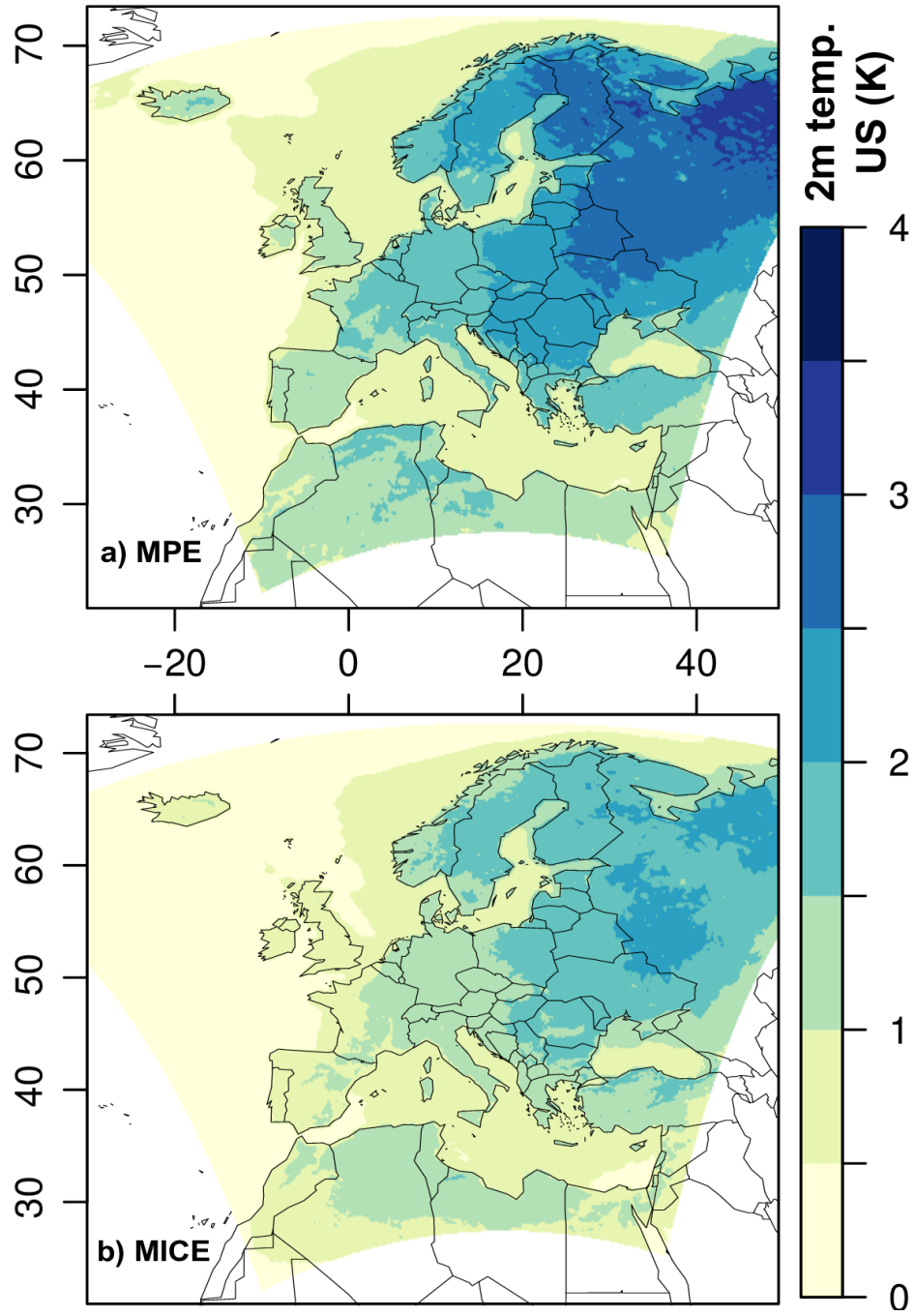


Figure 8: Spatial distribution of the inter-member variance for surface temperature (K) in EUR-15 domain of experiment B (year 1999). a) multi-physics ensemble. b) multi-initial-conditions ensemble.

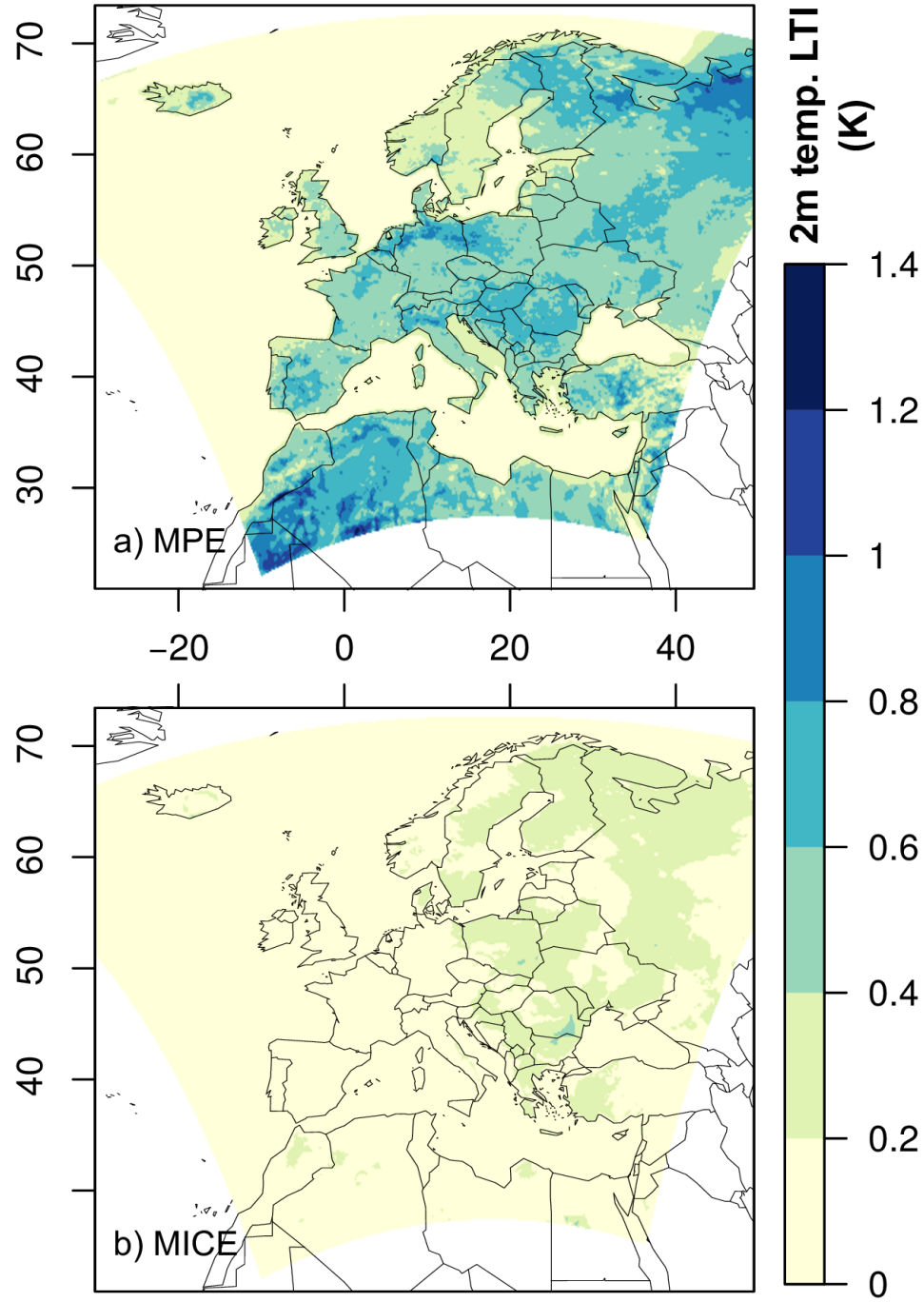


Figure 9: Long-term impact of multi-physics (a) and multi-initial-conditions (b) on surface temperature (K).